A Population of Compact Elliptical Galaxies Detected with the Virtual Observatory

Igor Chilingarian[1,2,3*], Véronique Cayatte[4], Yves Revaz[5], Serguei Dodonov[6], Daniel Durand[7], Florence Durret [8,9], Alberto Micol[10] & Eric Slezak[11]

[1] Observatoire de Paris-Meudon, LERMA, UMR 8112,
61 Av. de l'Observatoire, 75014 Paris, France
[2] Sternberg Astronomical Institute, Moscow State University,
13 Universitetsky prospect, Moscow, 119296, Russia
[3] Observatoire de Paris, VO Paris Data Centre,
61 Av. de l'Observatoire, 75014 Paris, France
[4] Observatoire de Paris-Meudon, LUTH, UMR 8102,
5 pl. Jules Janssen, 92195 Meudon, France
[5] Ecole Polytechnique Fédérale de Lausanne, Laboratory of Astrophysics,
51. Ch. des Maillettes, 1290 Sauverny, Switzerland
[6] Special Astrophysical Observatory, Nizhnij Arkhyz,
Zelenchukskij region, Karachai-Cirkassian Republic, 369167, Russia
[7] National Research Council Canada, Herzberg Institute of Astrophysics,
5071 W. Saanich Rd, Victoria, BC, Canada V9E 2E7
[8] CNRS, UMR 7095, Institut d'astrophysique de Paris,
[9] UPMC Université Paris 06, UMR 7095, Institut d'Astrophysique de Paris,
98bis, boulevard Arago, 75014 Paris, France
[10] European Southern Observatory,
Karl-Schwarzschild-Strasse 2, 85748 Garching bei Munchen, Germany
[11] University of Nice Sophia Antipolis, CNRS, Observatoire de la Côte d'Azur,
B.P. 4229, 06304 Nice Cedex 4, France

*To whom correspondence should be addressed; E-mail: igor.chilingarian@obspm.fr

Compact elliptical galaxies are characterized by small sizes and high stellar densities. They are thought to form through tidal stripping of massive progenitors. However, only a handful of them were known, preventing us from understanding the role played by this mechanism in galaxy evolution. We present a population of 21 compact elliptical galaxies gathered with the Virtual Observatory. Follow-up spectroscopy and data mining, using high resolution images and large databases, show that all the galaxies exhibit old metal-rich stellar populations different from those of dwarf elliptical galaxies of similar masses but similar to those of more massive early-type galaxies, supporting the tidal stripping scenario. Their internal properties are reproduced by numerical simulations, which result in compact dynamically hot remnants resembling the galaxies in our sample.

Present-day clusters of galaxies host rich populations of dwarf elliptical (dE) and lenticular (dS0) galaxies (*1*) having regular morphology and lacking ongoing star formation and interstellar medium (ISM). These galaxies are thought to form by internal processes such as supernova feedback to the star formation (*2*), or external agents [ram pressure stripping by hot intergalactic gas (*3*) and/or gravitational harassment (*4*)] acting on gas-rich progenitors. Tidal stripping had not been considered as an important mechanism governing galaxy formation until the recent discovery of ultra-compact dwarf galaxies (*5,6*) (UCD), i.e. very compact stellar systems several times more massive than known globular clusters. However, UCDs ($L \sim 10^7 L_\odot$) are about two orders of magnitude less luminous than bright dEs and, therefore, can be studied in only a handful of nearby galaxy clusters.

Compact elliptical (cE), or $M32$-like galaxies, which are also thought to form through tidal stripping (*7*), have luminosities ($\sim 10^9 L_\odot$ (*8–11*)) similar to those of dEs, whereas their half-light radii ($R_e \sim 0.25$ kpc) are several times smaller resulting in much higher mean surface

brightness ($\langle\mu\rangle_e$) values compared to dEs. These two criteria are easy to formalize and apply to members of nearby galaxy clusters at known distances, hence having a known spatial scale. Ground-based optical telescopes cannot resolve objects the size of 0.25 kpc beyond 50 Mpc. To find them in clusters out to 200 Mpc, thus increasing by a factor of 60 the volume of the nearby Universe where cEs remain spatially resolved, it is necessary to use the Hubble Space Telescope (HST).

We created a workflow, i.e. an automatic data retrieval and analysis system to search for cE galaxies in large data collections provided by the Virtual Observatory (VO, (*12*)). It comprised the following steps. (i) Identify nearby galaxy clusters at redshifts $z < 0.055$ using the Vizier Service (*13*) at the Centre de Données Astronomiques de Strasbourg. Without this condition our potential candidate cE galaxies would have been too faint for spectroscopic follow-up. (ii) Once the sources were identified, gather more precise measurements using other VO services including the NASA/IPAC Extragalactic Database (NED, (*14*)). (iii) Use the IVOA Simple Image Access Protocol to find and fetch the HST images of selected galaxy clusters from the Hubble Legacy Archive (HLA, (*15*)). (iv) For each image, run the SExtractor source identification software (*16*) to obtain half-light radii, total luminosities and approximate light profiles for all galaxies in each frame. (v) Apply color corrections to homogenize the results for all photometric bands and use the surface brightness – half-light radius criteria to find cE candidates. (vi) Finally, query NED, Vizier and a database of Sloan Digital Sky Survey Data Release 7 (*17*) to find additional information for candidate objects, such as published redshifts and integrated photometry.

Having applied the workflow to the entire HST Wide-Field Planetary Camera-2 (WFPC2) data collection in the HLA we ended up with archival images of 63 clusters with 55 candidate cE and tidally stripped elliptical galaxies in 26 of them.

Our workflow, which uses only imaging data, may confuse cE galaxies with (i) foreground

or cluster compact star-forming galaxies; (ii) background giant early-type galaxies hosting bright active nuclei (AGN); (iii) background post-starburst galaxies. Star-forming galaxies can be discriminated automatically through their blue colors if multi-band data are available, or by eye, examining their clumpy morphology. The two other cases may arise when the distance to the background object is 2–3 times the distance to the cluster, i.e. $<$400–500 Mpc ($z < 0.12$) in our study. The probability of having a post-starburst galaxy at this redshift is very low (*18*) and AGNs can be ruled out by checking X-ray point source catalogues.

We immediately confirmed the nature of 14 cE galaxies (see Fig. 1). For 6 of them, where archival SDSS DR7 spectra were available, we derived their physical properties: internal kinematics and stellar populations. For the other 8 candidate galaxies, we obtained redshifts from the literature through the NED and Vizier services.

To increase the sample of confirmed cE galaxies, we observed three of the galaxy clusters, Abell 160, Abell 189, and Abell 397, hosting 7 candidate galaxies altogether having $2.3 \cdot 10^8 < L_B < 1.1 \cdot 10^9 L_\odot$. This was done with the multi-slit unit of the SCORPIO spectrograph (*19*) at the Russian 6-m "Big Telescope Alt-azimuthal" in August 2008 (SOM). The spectra were fit with high-resolution stellar population models using the NBURSTS full spectral fitting technique (*20*) (SOM), obtaining precise radial velocities, internal velocity dispersions, luminosity-weighted stellar ages and metallicities. All 7 candidate objects were confirmed to be cluster members having global internal velocity dispersions between 50 and 100 km s^{-1} and old stellar populations. One of them exhibits a possible tidal feature (Fig. 2).

None of the 21 cE galaxies in our sample (summarized in Tables S1, S2) exhibits a young stellar population. The luminosity-weighted metallicities are between $Z_\odot/2.5$ ([Fe/H] $= -0.4$ dex) and the solar value for all galaxies except for ACO 189 J012325.96+014236.2 where it is as low as $Z_\odot/5$. Three galaxies are offset by $> +0.3$ dex from the luminosity-metallicity relation for early-type galaxies (Fig. 1, bottom); three others reside +0.2 to +0.3 dex above it. The internal

velocity dispersions are close to the values expected for the Faber-Jackson (*21*) relation and systematically above those of dEs. All these properties support the scenario where cE galaxies are created through tidal stripping of intermediate-luminosity disc galaxies.

Tidal stripping of an early-type disc galaxy should primarily affect its extended disc. Its centrally concentrated bulge should be able to survive even severe tidal interactions. After dynamical relaxation, a tidally-stripped remnant may slightly expand, decreasing its stellar velocity dispersion. For ISM-deficient galaxies, such as early-type systems in clusters, tidal stripping will not change the overall age and metallicity of their stars, but the total stellar mass will be significantly reduced. Because there is a relation between mean metallicities and stellar masses of galaxies (*22*, *23*), this process will create objects with uncommon stellar populations; i.e. systems that are too metal-rich for their observed stellar masses, corresponding to what we see in galaxies populating the central region of the Abell 496 cluster (*24*) and in UCDs (*25*).

The stellar metallicity can also be increased by star formation induced by external sources, e.g. by mergers or encounters with gas-rich galaxies where tidal compression may significantly increase the star formation efficiency (*26*). However, in this case the mean age of the stellar population would decrease because newly formed stars have much lower mass-to-light ratios in the optical than older populations do, contributing significantly to the total light, even with low mass fractions. All the galaxies in our sample exhibit old populations, hence ruling out this scenario.

Tidal effects must be stronger in the vicinities of massive galaxies, in particular around cluster dominant galaxies (cD).

To study the efficiency of tidal stripping we simulated the interaction of a disc galaxy with a galaxy cluster potential using the GADGET-2 code (*27*) (SOM for further details). We explored the tidal stripping effects at a spatial resolution (~ 100 pc) several times higher than that of typical simulations of galaxy clusters, checking 32 different orbital configurations. We converted

the stellar density maps produced by our simulations into surface brightness and processed them using the SExtractor software in the same way as we did for the search of cE galaxies in HST images.

Our simulations demonstrate the efficiency of tidal stripping in reducing the stellar mass of a disc galaxy. Even in case of quasi-circular orbital configurations, the large-scale stellar disc was heavily stripped, decreasing the galaxy stellar mass by a factor of 2 (Fig. 3) on a timescale of 600–700 Myr. We compared the evolution of total magnitude, surface brightness and internal velocity dispersion of a stripped galaxy to observations (Fig. 1, top and middle panels). Interactions on radial orbits resulted in heavier mass loss of up-to 90 per cent, although a remnant became quickly accreted by a cD galaxy. Presumably, by scaling down the systems in mass, i.e. by replacing a giant disc with a low-luminosity or dwarf S0, it should be possible to reproduce the formation of UCD and transitional cE/UCD (*11, 28*) galaxies.

In our study we used Virtual Observatory data mining to convert the class of cE galaxies from "unique" into "common in certain environmental conditions", i.e. more frequent than was previously thought. We confirmed the nature of 21 galaxies selected by the VO workflow with follow-up observations and archival data. We also reproduced their properties with numerical simulations. We can confirm that tidal stripping of the stellar component plays an important role in the morphological transformation of galaxies in dense environments, producing remnants spanning a luminosity range of four orders of magnitude.

References and Notes

1. H. C. Ferguson, B. Binggeli, Astron. Astrophys. Rev. **6**, 67 (1994).

2. A. Dekel, J. Silk, Astrophys. J. **303**, 39 (1986).

3. J. E. Gunn, J. R. I. Gott, Astrophys. J. **176**, 1 (1972).

4. B. Moore, N. Katz, G. Lake, A. Dressler, A. Oemler, Nature **379**, 613 (1996).

5. S. Mieske, M. Hilker, L. Infante, Astron. Astrophys. **383**, 823 (2002).

6. M. J. Drinkwater, *et al.*, Nature **423**, 519 (2003).

7. K. Bekki, W. J. Couch, M. J. Drinkwater, M. D. Gregg, Astrophys. J. **557**, L39 (2001).

8. A. W. Graham, Astrophys. J. **568**, L13 (2002).

9. S. Mieske, *et al.*, Astron. Astrophys. **430**, L25 (2005).

10. I. Chilingarian, *et al.*, Astron. Astrophys. **466**, L21 (2007).

11. J. Price, *et al.*, Mon. Not. R. Astron. Soc. **397**, 1816 (2009).

12. The Virtual Observatory is a realization of an e-Science concept in astronomy with an emphasis on data mining, where data archives and software tools interoperate using a set of peer-reviewed standards and technologies developed by the International Virtual Observatory Alliance (IVOA, http://www.ivoa.net/). It forms a virtual environment aimed at facilitating astronomical research and increasing scientific output of data by providing transparent access to catalogues, databases, archives, data visualization, processing and analysis tools.

13. http://vizier.u-strasbg.fr/.

14. http://nedwww.ipac.caltech.edu/.

15. http://hla.stsci.edu/.

16. E. Bertin, S. Arnouts, Astron. Astrophys. Suppl. Ser. **117**, 393 (1996).

17. K. N. Abazajian, *et al.*, Astrophys. J. Suppl. Ser. **182**, 543 (2009).

18. T. Goto, R. C. Nichol, S. e. a. Okamura, PASJ **55**, 771 (2003).

19. V. L. Afanasiev, A. V. Moiseev, *Astronomy Letters* **31**, 194 (2005).

20. I. Chilingarian, P. Prugniel, O. Sil'chenko, M. Koleva, *Stellar Populations as Building Blocks of Galaxies*, A. Vazdekis, R. R. Peletier, eds. (Cambridge University Press, Cambridge, UK, 2007), vol. 241 of *IAU Symposium*, pp. 175–176.

21. S. M. Faber, R. E. Jackson, Astrophys. J. **204**, 668 (1976).

22. A. Gallazzi, S. Charlot, J. Brinchmann, S. D. M. White, C. A. Tremonti, Mon. Not. R. Astron. Soc. **362**, 41 (2005).

23. A. Renzini, Annu. Rev. Astron. Astrophys. **44**, 141 (2006).

24. I. V. Chilingarian, *et al.*, Astron. Astrophys. **486**, 85 (2008).

25. I. V. Chilingarian, V. Cayatte, G. Bergond, Mon. Not. R. Astron. Soc. **390**, 906 (2008).

26. E. Emsellem, G. van de Ven, Astrophys. J. **674**, 653 (2008).

27. V. Springel, Mon. Not. R. Astron. Soc. **364**, 1105 (2005).

28. I. V. Chilingarian, G. A. Mamon, Mon. Not. R. Astron. Soc. **385**, L83 (2008).

29. B. Binggeli, H. Jerjen, Astron. Astrophys. **333**, 17 (1998).

30. I. V. Chilingarian, Mon. Not. R. Astron. Soc. **394**, 1229 (2009).

31. R. Bender, D. Burstein, S. M. Faber, Astrophys. J. **399**, 462 (1992).

32. This study is based on observations made with the NASA/ESA Hubble Space Telescope, and obtained from the Hubble Legacy Archive, which is a collaboration between the Space

Telescope Science Institute (STScI/NASA), the Space Telescope European Coordinating Facility (ST-ECF/ESA) and the Canadian Astronomy Data Centre (CADC/NRC/CSA); observations collected with the 6-m telescope of the Special Astrophysical Observatory (SAO) of the Russian Academy of Sciences (RAS) operated under the financial support of the Science Department of Russia (registration number 01-43). The simulations were run on the Callisto cluster at the École Polytechnique Fédérale de Lausanne (EPFL) and on the Regor cluster of the Geneva Observatory. This research made use of SAOImage DS9 developed by Smithsonian Astrophysical Observatory, Aladin developed by the Centre de Données Astronomiques de Strasbourg, "exploresdss" script by G. Mamon; the VizieR catalogue access tool, CDS, Strasbourg, France, and the NASA/IPAC Extragalactic Database (NED) operated by the Jet Propulsion Laboratory, California Institute of Technology, under contract with the National Aeronautics and Space Administration. Funding for the SDSS and SDSS-II has been provided by the Alfred P. Sloan Foundation, the Participating Institutions, the National Science Foundation, the U.S. Department of Energy, the National Aeronautics and Space Administration, the Japanese Monbukagakusho, the Max Planck Society, and the Higher Education Funding Council for England. The SDSS Web Site is http://www.sdss.org/. The simulation data analysis and galaxy maps were done using the parallelized Python pNbody package (http://obswww.unige.ch/∼revaz/pNbody/). This work was supported by the Swiss National Science Foundation. IC acknowledges additional support from the RFBR grant 07-02-00229-a. Special thanks to F. Combes and G. Mamon for useful discussions and suggestions and to R. Trilling who kindly agreed to edit the manuscript. The content of the workflow and its explicit description are available on the web-pages of the VO Paris Data Centre (http://vo-web.obspm.fr/) and the European Virtual Observatory EURO-VO.

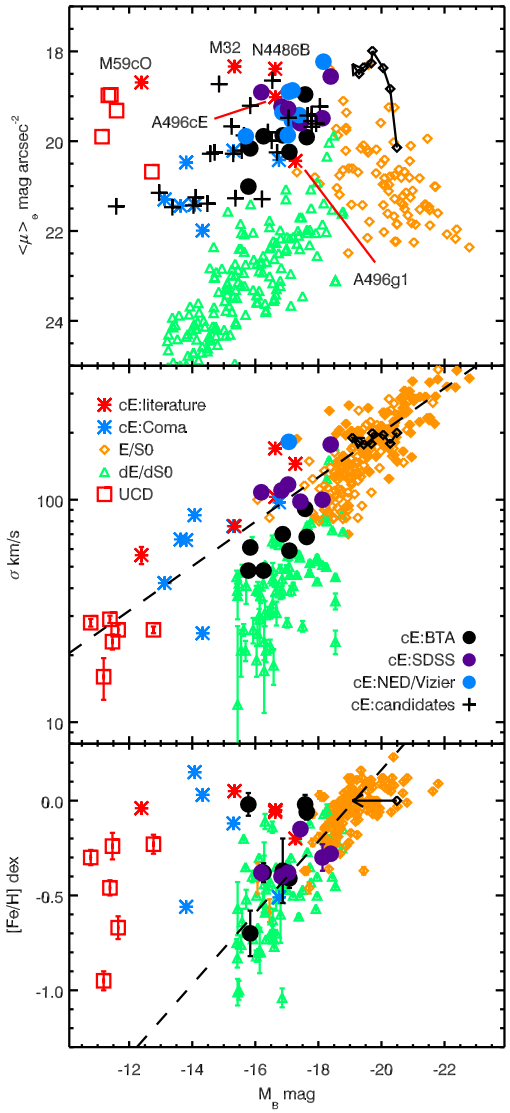

Figure 1: Structure, dynamics and stellar populations of early-type galaxies. Mean surface brightness within a half-light radius $\langle\mu\rangle_e$ (top panel), global stellar velocity dispersion σ (middle panel) and metallicity [Fe/H] (bottom panel) of galaxies are displayed as a function of the B-band absolute magnitudes. The confirmed tidally stripped galaxies are displayed with filled circles of black, violet and blue colours for BTA-spectroscopy, SDSS-spectroscopy, and literature redshifts from NED or Vizier, respectively. Crosses denote the candidate cE galaxies without spectroscopic confirmation. Red asterisks are for known compact elliptical galaxies, blue asterisks are for recently discovered compact stellar systems in the Coma cluster (*11*). The dashed lines in the middle and bottom panel show the Faber-Jackson (*21*) and luminosity-metallicity (*25*) relations. Literature data (dE/dS0 galaxies (*24,29,30*), intermediate-luminosity and giant early-type galaxies (*31*), UCDs (*25*)) are complemented with the data for 140 early-type galaxies in the Coma cluster from the SDSS DR7 spectra obtained with the NBURSTS technique (SOM). All metallicity measurements shown in the bottom panel, except those of Coma compact stellar systems, are homogeneous as they were obtained using the same data analysis technique. Black path displays the evolution of a simulated barred early-type spiral tidally stripped by the cluster potential on a quasi-circular orbit (SOM) followed for 2 Gyr.

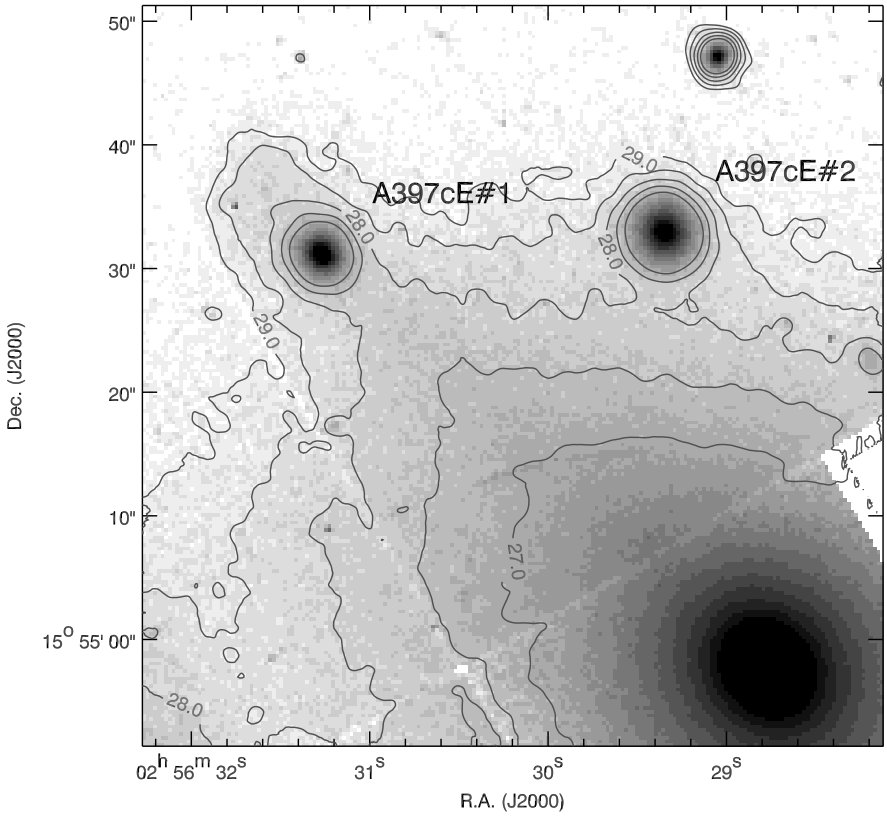

Figure 2: Fragment of a WFPC2 HST image of the central region of Abell 397 obtained from the HLA with two candidate cE galaxies; north is up, east is left. The overplotted isophotes correspond to surface brightness levels from 29.0 to 27.0 mag arcsec^{-2} in the $F814W$ band with 0.5 mag arcsec^{-2} interval. A397cE#1 exhibits a prominent extended low surface brightness feature toward the north-east, probably originating from its tidal interaction with the cluster dominant galaxy UGC 2413 in the lower-right corner.

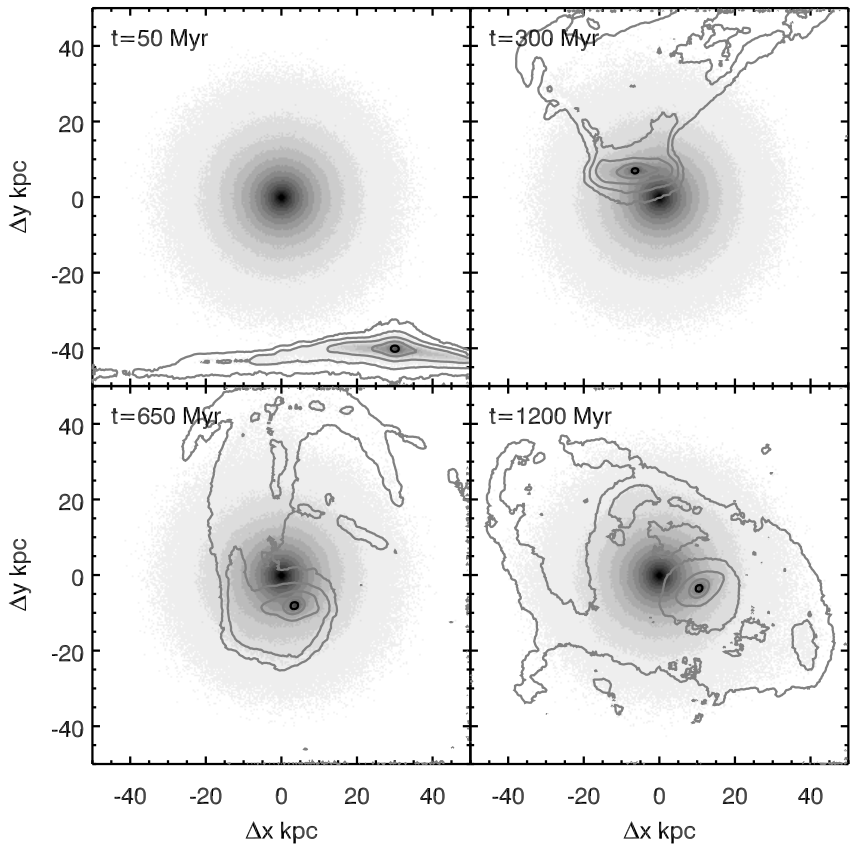

Figure 3: Numerical simulations of the tidal stripping of an intermediate-luminosity barred disc galaxy. The panels display four snapshots of an N-body simulation of the tidal disruption of a barred disc galaxy, initially on a quasi-circular orbit, by the cluster cD galaxy shown in the centre. The disc galaxy plane is perpendicular to the initial orbital plane. Each panel is 100×100 kpc in size, the density scale is logarithmic. The density contours (every 2 mag arcsec^{-2}) are displayed for the stars which initially belonged to the disc galaxy. The simulations demonstrate how the outer disc of a galaxy gets stripped leaving a compact remnant and stripped material in arcs and tails.

Supporting online material

Observations, data reduction and analysis

We observed three galaxy clusters (Abell 160, Abell 189, and Abell 397), hosting 7 candidate galaxies altogether ($-17.1 < M_B < -15.4$ mag) with the SCORPIO (Spectral Camera with Optical Reducer for Photometric and Interferometric Observations) spectrograph (*19*) at the Russian 6-m "Big Telescope Alt-azimuthal" during one observing run on the nights of 25th, 27th, and 28th of August 2008 (observational programme "Kinematics and stellar populations of newly discovered compact elliptical galaxies", P.I.:IC). We used the multi-slit mode of the instrument and the VPHG2300g grism centered at 5250 Å. This allowed us to observe up to 16 galaxies simultaneously in every 6×6 arcmin field of view, with a spectral resolution of about $R = 2200$ (FWHM = 2.4 Å), using 1.2 arcsec-wide 18 arcsec-long interactively placed slitlets, controlled by electromagnets in the focal plane of the focal reducer. The total exposure times were 3600, 6000, and 3000 s for Abell 160, Abell 189, and Abell 397 respectively. Atmospheric seeing quality was between 1.3 and 2.5 arcsec most of the time, therefore the observed cE galaxies remained spatially unresolved.

The calibrations obtained during the observing run included: (i) bias frames, (ii) arc line spectra of He-Ne-Ar, (iii) internal spectral flat fields, (iv) observations of spectrophotometric standard stars, (v) high signal-to-noise twilight spectra obtained in each configuration of the multi-slit block.

We reduced the data using the ITT IDL software package. The primary data reduction steps comprising bias subtraction, flat fielding, Laplacian filtering (*33*) for removing cosmic-ray hits were applied to all science and calibration frames. We then traced the slitlet positions using flat-field spectra, estimated the cross-dispersion geometrical distortions and corrected for them using two-dimensional polynomial warping. Then, for every individual slitlet we built

the wavelength solution by identifying arc lines and fitting their positions with two-dimensional polynomial of the 3rd order in both dimensions, along and across dispersion, and linearized the spectra. The obtained wavelength solutions had fitting residuals of about 0.1 Å RMS mostly due to the statistical errors in determined arc line positions. These positions were taken into account later in the data analysis step. Error frames were computed using the photon statistics and processed through the same reduction steps as the data.

In order to precisely measure stellar velocity dispersions, it is essential to take into account systematic errors in the obtained wavelength solutions and to get precise information about the spectral resolution variations along and across dispersion. To do this, we fitted the high-resolution ($R = 10000$) solar spectrum against the linearized twilight spectra in five wavelength segments overlapping by 20 per cent, covering the spectral range of the SCORPIO setup using the penalized pixel fitting procedure (*34*).

We then extracted one-dimensional spectra of the cE candidate galaxies from the corresponding slitlets and subtracted the night sky emission spectrum reconstructed from regions of the same slitlets not including the target galaxies. In the case of Abell 397, we took into account the contamination of the ACO 397 J025631.27+155531.2 (A397cE1) spectrum by the cD galaxy by creating a background spectrum from the part of the slitlet covering the region of the cD. This was symmetric along the major axis to that where the A397cE1 galaxy is projected. We analysed independently all the one-dimensional spectra obtained.

We used the NBURSTS full spectral fitting technique (*20*) with high-resolution ($R = 10,000$) PEGASE.HR (*35*) simple stellar population (SSP) models to extract kinematics and stellar populations from our spectra. The fitting procedure comprised the following steps: (i) a grid of SSP spectra with a fixed set of ages (spaced nearly logarithmically from 20 Myr to 18 Gyr) and metallicities (from -2.0 to $+0.5$ dex) was convolved with the wavelength-dependent instrumental response of SCORPIO obtained from the analysis of twilight frames (*36*); (ii) a non-linear

least square fitting against the observed spectrum was done for a template picked from the pre-convolved SSP grid interpolating on age ($\log t$), and metallicity (Z). It was broadened according to the line-of-sight velocity distribution (LOSVD) parametrized by v and σ and multiplied pixel by pixel with an $n^{\rm th}$ order Legendre polynomial (multiplicative continuum). This resulted in $n+5$ parameters to be determined (we used $n=10$ for our SCORPIO data). BTA spectra with their best-fitting templates are shown in Fig S3.

It was shown (*30*), that more optimal usage of information contained in absorption line spectra using full spectral fitting techniques, improved the precision of age and metallicity estimates by a factor of a few, as compared to individual absorption line strength indices. This explains the low statistical uncertainties on the stellar population parameters presented in Tables S1–S2. It was also demonstrated (*24, 25, 36*) that velocity dispersion measurements remain precise down to at least 1/2 of the instrumental spectral resolution. It was also shown that stellar population measurements remain unbiased for the non-solar α/Fe element abundance ratio. However, as any other stellar population analysis technique, NBURSTS produces model-dependent results which may be systematically different if one uses different stellar population models. All data points in Fig. 1, except those representing Coma compact stellar systems (*11*) were obtained using the NBURSTS spectral fitting technique with the same stellar population models. It is therefore correct to compare them. We did not have the original spectra for the Coma compact stellar systems, therefore the published age and metallicity values (*11*) were used.

We applied the same fitting technique to available SDSS DR7 spectra of 6 candidate cE galaxies using the wavelength-dependent spectral resolution information provided for every individual dataset by the SDSS archive. We similarly fitted 140 SDSS DR7 spectra of early-type galaxies in the central region of the Coma cluster (Abell 1656) in order to build the Faber–Jackson (*21*) and luminosity–metallicity relations for intermediate-luminosity and giant galaxies displayed in Fig. 1.

Results

In Fig. S1 we provide HST WFPC2 images for all confirmed cE galaxies. For each galaxy we display: (a) the full WFPC2 field of view often containing a bright cluster galaxy or a cD galaxy and (b) a zoomed cutout featuring the cE galaxy corresponding to a spatial size of 5×5 kpc at the cluster distance.

In Tables S1–S2 we present the photometric, kinematic, and stellar population properties of cE galaxies with confirmed cluster membership. The columns in Table S1 provide (from left to right): record numbers, cluster number in the Abell catalogue (*37*), cluster heliocentric radial velocities from NED, IAU-recommended names, absolute B-band magnitudes, half-light radii, mean surface brightnesses within r_e and ellipticities of the cE galaxies. In Table S2 for each cE galaxy we provide: projected distances from the cD galaxies, heliocentric radial velocities, stellar velocity dispersions, luminosity weighted ages and metallicities, and sources of redshift and photometric data (absolute magnitude and effective surface brightness). The half-light radii r_e, and ellipticities in Table S1 are always measured from HST WFPC2 imaging, using the SExtractor software (*16*), while the sources of total magnitudes vary. We give preference to the ground-based data (SDSS, CADC MegaPipe Stacks) if their photometric bandpass is closer to the B-band than the HST bandpass. We apply colour transformations (*38*) assuming an elliptical galaxy spectrum, in order to convert measurements into the B band. Corresponding mean surface brightnesses $\langle\mu\rangle_{e,B}$ are computed from the HST WFPC2 measured half-light radii and adopted B-band magnitudes; flat colour profiles are assumed. All magnitude and surface brightness values are corrected for Galactic extinction (*39*) and K-corrections. The surface brightness values are additionally corrected for cosmological dimming.

In addition to the galaxies presented in Tables S1,S2, our workflow re-detected two objects in the Abell 496 cluster which were referenced before as A496cE and A496g1 (*10*). They

are shown as known cE galaxies in Fig. 1, but we have intentionally removed them from Tables S1,S2.

N-body simulations of tidal stripping

Spatial resolution of cosmological simulations is insufficient to resolve the internal structure of intermediate luminosity galaxies in detail. A number of studies addressed dynamical and morphological evolution of disc galaxies in clusters from simulations (*4*, *40–42*); however, none of them analyzed strong tidal stripping and tidal disruption. The nature of Messier 32, the prototypical cE galaxy, was explained by tidal threshing (*7*) but it was not shown how this process would act on progenitors having larger masses in a cluster environment. This motivated us to perform 32 dedicated intermediate-resolution (~ 100 pc) N-body simulations of interactions of a disc galaxy with a galaxy cluster potential using the GADGET-2 treecode (*27*). We only considered the gravitational forces, neglecting the ram pressure stripping effects.

The disc galaxy is based on the "classical model" (*43*). It is made from a bulge ($0.42 \times 10^{11}\,\mathrm{M}_\odot$), a Miyamoto–Nagai (*44*) gaseous disc ($0.3 \times 10^{11}\,\mathrm{M}_\odot$), an exponential stellar disc ($1.04 \times 10^{11}\,\mathrm{M}_\odot$) and a Plummer dark matter halo ($8.9 \times 10^{11}\,\mathrm{M}_\odot$). The relative masses of all components are set, such as the rotation curve being flat up to 40 kpc. The total mass is $9.6 \times 10^{11} M_\odot$. As an initial condition, we took a disc containing a central bar. The extension of the stellar bar is about 4 kpc with an axial ratio $a/b = 1.8$. Its rotation period is 220 Myr ($\Omega_p = 28$ km s^{-1} kpc^{-1}) placing the inner Lindblad resonance at 3.5 kpc and the corotation radius at 8.4 kpc.

The galaxy cluster potential model is based on the data of Messier 87 (*45*), the Virgo cluster cD. It is modeled by a live NFW (*46*) potential represented by 5×10^5 particles with a concentration of 7 kpc and a virial mass of 1.4×10^{14} M$_\odot$. We also took into account the central giant black hole of 3×10^9 M$_\odot$, represented by a Plummer sphere with a core of 100 pc, which is

similar to the resolution of our simulations.

We performed 32 simulations varying the orbital angular momentum (initial tangential velocities of 650, 180, 120, and 50 km s^{-1} corresponding to initial ellipticities of 0.04, 0.79, 0.86, and 0.94) and the disc inclination with respect to the orbital plane (0, $\pm$45, $\pm$90, $\pm$135, and 180 deg). Each simulation was followed for 2 Gyr. Initially the disc galaxy was located 50 kpc from the centre of the cD potential.

The surface density maps presented in Fig. 3 are computed from the stellar components by adding the cD stellar density profile. It was modelled by fitting the light distribution of Messier 87 (*47*) with a Hernquist (*48*) profile and assuming constant mass-to-light ratio along the radius. The outermost contour corresponds to the B-band surface brightness value $\mu_B = 28$ mag arcsec^{-2}. The contours are shown with a step of 2 mag arcsec^{-2}.

In Fig. 1 we present the evolution of structural and dynamical properties of a stripped galaxy. We took initial ages of 4 and 10 Gyr for the bulge and disc components. We computed at every timestep the corresponding mass-to-light ratios from the PEGASE.2 stellar population models (*49*) in order to convert surface density into B-band surface brightness. The resulting maps were analyzed by the SExtractor software in the same way as the HST images, which we used to search for cEs in galaxy clusters. The black path displays the initial conditions and snapshots at 50, 250, 500, 750, 1200, 1500, and 1950 Myr.

Our simulations demonstrate that the large-scale stellar discs get heavily stripped even on the quasi-circular orbit ($e = 0.04$) 600–800 Myr after the start of the simulation. About 50 per cent of the initial stellar mass of the galaxy is stripped. However, since only the disc, having lower mass-to-light ratio than the bulge is affected, the total predicted B-band luminosity decreases by more than a factor of 3.

The progenitor's bar remains weakly affected and looks structurally like a high surface brightness flattened elliptical galaxy resembling ACO496 J043336.12-131442.5. In case of high

disc inclination to the initial orbital plane, at certain moments in time, the remnant's major axis becomes nearly parallel to the line of sight, creating the effect of very high surface brightness round galaxies. On such a quasi-circular orbit, the stripped remnant may remain for quite a long time without further significant mass loss. We note that the tidal stripping scenario is compatible with the low-surface brightness outer exponential discs detected in Messier 32 (*8*) and A496cE (*10*).

Interactions on radial orbits ($e = 0.86 \ldots 0.94$) result in more efficient stripping with a stellar mass loss reaching 85–90 per cent 600–700 Myr after the start of the simulation. The first 70–75 per cent are already lost at t =250–300 Myr. The outer isophotes of the remnant may become rounder due to the interplay between tidal compression in the tangential directions and rotation of the barred galaxy. Correspondingly, the remnant's mean surface density changes periodically, being connected to the orbital motion. However, in all cases of radial orbits, the remnants are already accreted by the cD galaxy at t =1.0–1.2 Gyr.

Thus, we have two alternatives: (i) galaxies on quasi-circular orbits may remain for a long time without suffering significant structural changes after the initial stripping of their large-scale discs removing a significant fraction of the stellar mass; (ii) galaxies infalling on radial orbits lose mass more efficiently and over a shorter time. However, they are completely accreted by the cD on a timescale of about 1 Gyr, so one needs a supply of infalling galaxies on to the cluster centre in order to form cEs. Scaling the masses of progenitors, we can create compact galaxies ranging in luminosities. Given the dependence of the galaxy profile concentration on the luminosity (*50, 51*), one can expect lower central surface densities for tidally stripped galaxies originating from lower-mass progenitors.

A large fraction of the stripped material is not accreted by the cD galaxy and contributes to the diffuse intracluster light. Analysing its properties will help us to estimate the frequency of tidal stripping events and understand their importance as a mechanism of galaxy evolution in

dense environments.

Supporting References and Notes

33. P. G. van Dokkum, PASP **113**, 1420 (2001).

34. M. Cappellari, E. Emsellem, PASP **116**, 138 (2004).

35. D. Le Borgne, *et al.*, Astron. Astrophys. **425**, 881 (2004).

36. I. V. Chilingarian, P. Prugniel, O. K. Sil'chenko, V. L. Afanasiev, Mon. Not. R. Astron. Soc. **376**, 1033 (2007).

37. G. O. Abell, Astrophys. J. Suppl. Ser. **3**, 211 (1958).

38. M. Fukugita, K. Shimasaku, T. Ichikawa, PASP **107**, 945 (1995).

39. D. J. Schlegel, D. P. Finkbeiner, M. Davis, Astrophys. J. **500**, 525 (1998).

40. M. G. Abadi, B. Moore, R. G. Bower, Mon. Not. R. Astron. Soc. **308**, 947 (1999).

41. V. Quilis, B. Moore, R. Bower, *Science* **288**, 1617 (2000).

42. C. Mastropietro, *et al.*, Mon. Not. R. Astron. Soc. **364**, 607 (2005).

43. Y. Revaz, D. Pfenniger, F. Combes, F. Bournaud, Astron. Astrophys. **501**, 171 (2009).

44. M. Miyamoto, R. Nagai, PASJ **27**, 533 (1975).

45. E. Emsellem, *et al.*, Mon. Not. R. Astron. Soc. **352**, 721 (2004).

46. J. F. Navarro, C. S. Frenk, S. D. M. White, Astrophys. J. **490**, 493 (1997).

47. J. Kormendy, D. B. Fisher, M. E. Cornell, R. Bender, Astrophys. J. Suppl. Ser. **182**, 216 (2009).

48. L. Hernquist, Astrophys. J. **356**, 359 (1990).

49. M. Fioc, B. Rocca-Volmerange, Astron. Astrophys. **326**, 950 (1997).

50. L. Ferrarese, *et al.*, Astrophys. J. Suppl. Ser. **164**, 334 (2006).

51. A. W. Graham, R. Guzmán, Astron. J. **125**, 2936 (2003).

Table S1: Photometric properties of confirmed cE galaxies and their host clusters

N	Cluster	$cz_{\rm clus}$ km s^{-1}	IAU Name	M_B mag	r_e kpc	$\langle\mu\rangle_{e,B}$ mag arcsec^{-2}	ϵ
1	ACO 0160	13401	$J011257.62+152821.1$	-17.08	0.56	20.24	0.02
2	ACO 0160	13401	$J011258.85+152855.3$	-16.87	0.43	19.87	0.03
3	ACO 0160	13401	$J011300.24+152921.5$	-16.26	0.33	19.89	0.01
4	ACO 0189	9833	$J012325.96+014236.2$	-15.84	0.31	20.16	0.14
5	ACO 0189	9833	$J012326.58+014230.3$	-15.78	0.44	21.01	0.10
6	ACO 0397	9803	$J025629.35+155533.0$	-17.63	0.62	19.91	0.09
7	ACO 0397	9803	$J025631.27+155531.2$	-17.58	0.39	18.96	0.12
8	ACO 0400	7315	$J025744.50+060202.2$	-17.16	0.42	19.54	0.08
9	ACO 0496	9863	$J043336.12-131442.5$	-18.16	0.37	18.23	0.23
10	ACO 0496	9863	$J043338.55-131549.5$	-17.18	0.32	18.87	0.14
11	ACO 0779	6742	$J091947.87+334604.8$	-16.83	0.32	19.23	0.03
12	ACO 1177	9473	$J110947.06+214648.6$	-17.43	0.49	19.60	0.25
13	ACO 3526	3418	$J124853.91-411905.8$	-16.86	0.34	19.36	0.03
14	ACO 1656	6925	$J125923.41+275510.4$	-16.19	0.20	18.91	0.01
15	ACO 1656	6925	$J125942.30+275529.0$	-18.39	0.47	18.56	0.17
16	ACO 3558	14390	$J132758.71-312937.5$	-17.39	0.44	19.42	0.17
17	ACO 3562	14690	$J133340.86-314008.3$	-17.06	0.30	18.90	0.20
18	ACO 2040	13790	$J151250.26+072621.9$	-18.13	0.65	19.49	0.10
19	ACO 2052	10640	$J151641.28+070006.1$	-17.04	0.35	19.28	0.03
20	ACO 2634	9409	$J233825.48+270150.1$	-17.03	0.47	19.87	0.07
21	ACO 2634	9409	$J233829.31+270225.1$	-15.70	0.25	19.89	0.04

Table S2: Kinematics and stellar populations of confirmed cE galaxies

N	d_{proj}	v_r	σ	t	[Fe/H]	sources of redshifts
	kpc	km s^{-1}	km s^{-1}	Gyr	dex	and photometric data
1	66	12645 ± 4	59 ± 6	8.6 ± 2.8	-0.41 ± 0.05	z:BTA, ph:SDSS (g)
2	32	12549 ± 5	70 ± 6	16.2 ± 6.1	-0.37 ± 0.17	z:BTA, ph:SDSS (g)
3	11	12848 ± 4	48 ± 7	7.5 ± 2.2	-0.38 ± 0.05	z:BTA, ph:SDSS (g)
4	11	10019 ± 4	61 ± 7	17.5 ± 4.1	-0.70 ± 0.12	z:BTA, ph:HST ($F814W$)
5	6.6	10411 ± 3	48 ± 6	7.4 ± 2.2	-0.02 ± 0.06	z:BTA, ph:HST ($F814W$)
6	24	10278 ± 4	68 ± 5	9.0 ± 1.9	-0.06 ± 0.04	z:BTA, ph:CFHT (g)
7	33	10240 ± 4	91 ± 6	11.1 ± 2.6	-0.02 ± 0.05	z:BTA, ph:CFHT (g)
8	25	7790 ± 30	...	...	...	z:Vizier, ph:SDSS (g)
9	43	9415 ± 31	...	...	...	z:NED, ph:HST ($F555W$)
10	8.4	9814 ± 21	...	...	...	z:Vizier, ph:HST ($F555W$)
11	31	7142 ± 3	110 ± 4	12.0 ± 1.6	-0.40 ± 0.03	z:SDSS, ph:SDSS (g)
12	54	9250 ± 3	98 ± 4	9.6 ± 1.3	-0.15 ± 0.02	z:SDSS, ph:SDSS (g)
13	13	2317 ± 20	...	...	...	z:NED, ph:HST ($F555W$)
14	14	6925 ± 5	108 ± 4	11.2 ± 2.1	-0.38 ± 0.04	z:SDSS, ph:SDSS (g)
15	24	6916 ± 2	177 ± 2	12.7 ± 0.9	-0.28 ± 0.02	z:SDSS, ph:SDSS (g)
16	24	16668 ± 20	...	...	...	z:NED, ph:HST ($F814W$)
17	79	$14746 \pm ...$	182 ± 9	...	...	z:Vizier, ph:Vizier (B)
18	42	14551 ± 5	100 ± 7	13.0 ± 4.2	-0.30 ± 0.07	z:SDSS, ph:SDSS (g)
19	62	10350 ± 5	117 ± 6	10.0 ± 2.8	-0.38 ± 0.03	z:SDSS, ph:SDSS (g)
20	38	9532 ± 80	...	...	...	z:NED, ph:HST ($F555W$)
21	20	10183 ± 80	...	...	...	z:NED, ph:HST ($F814W$)

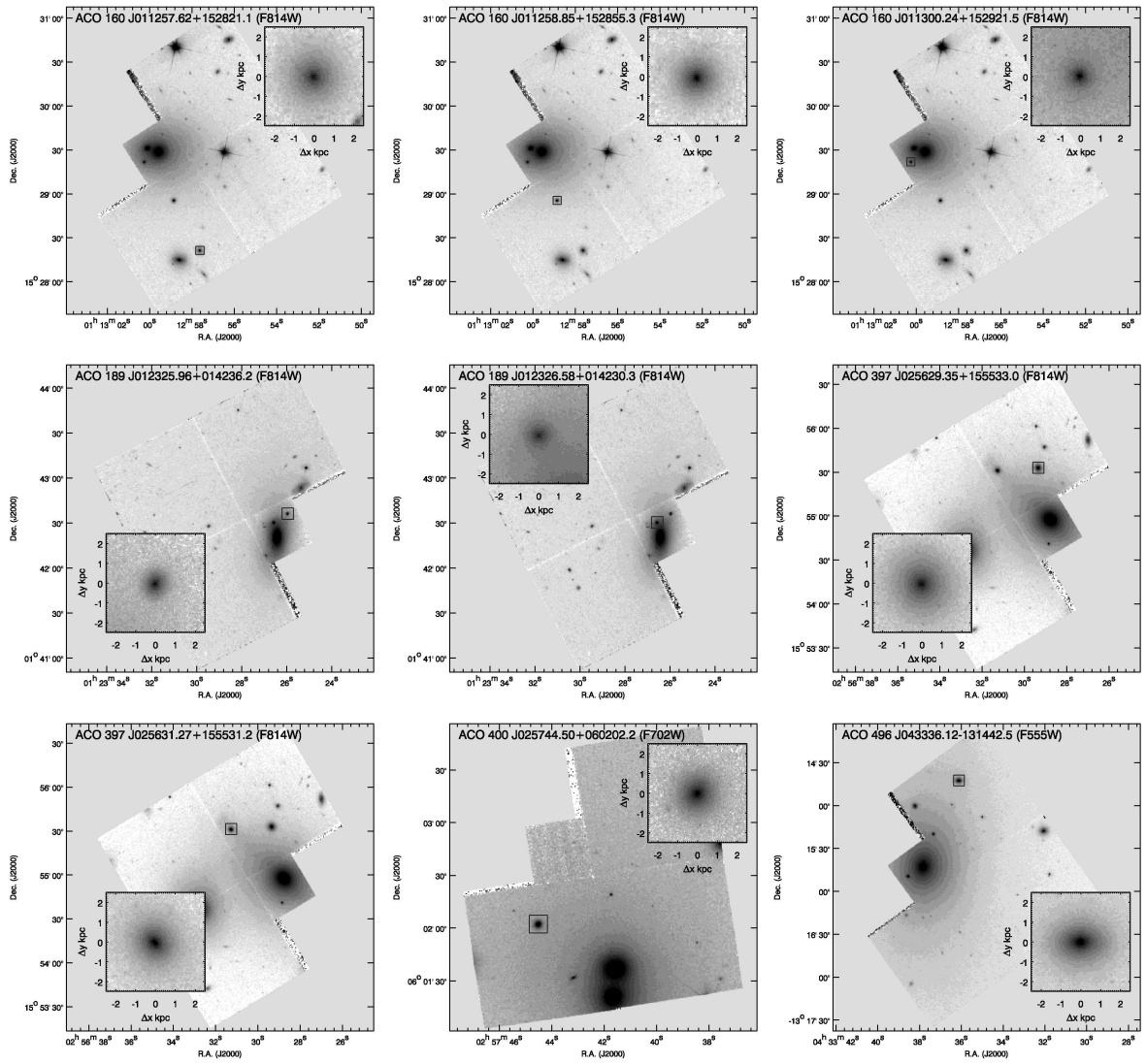

Figure S1: HST WFPC2 images of cE galaxies. For every galaxy we show the entire WFPC2 image and an inner panel displaying a 5×5 kpc region centered on the cE galaxy. Cluster identification, IAU recommended designation of the cE galaxy and the photometric bandpass are indicated.

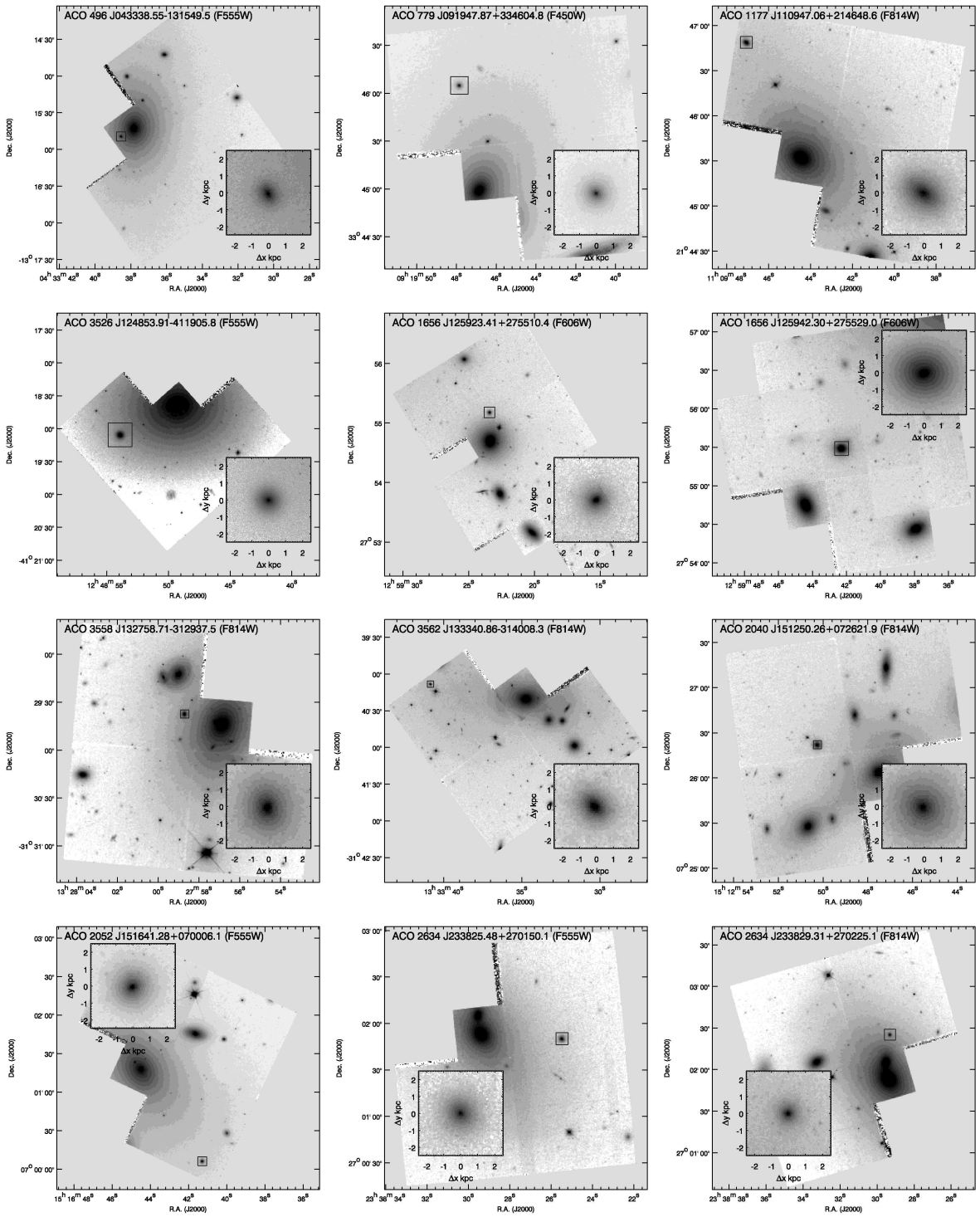

Figure S2: HST WFPC2 images of cE galaxies – contd.

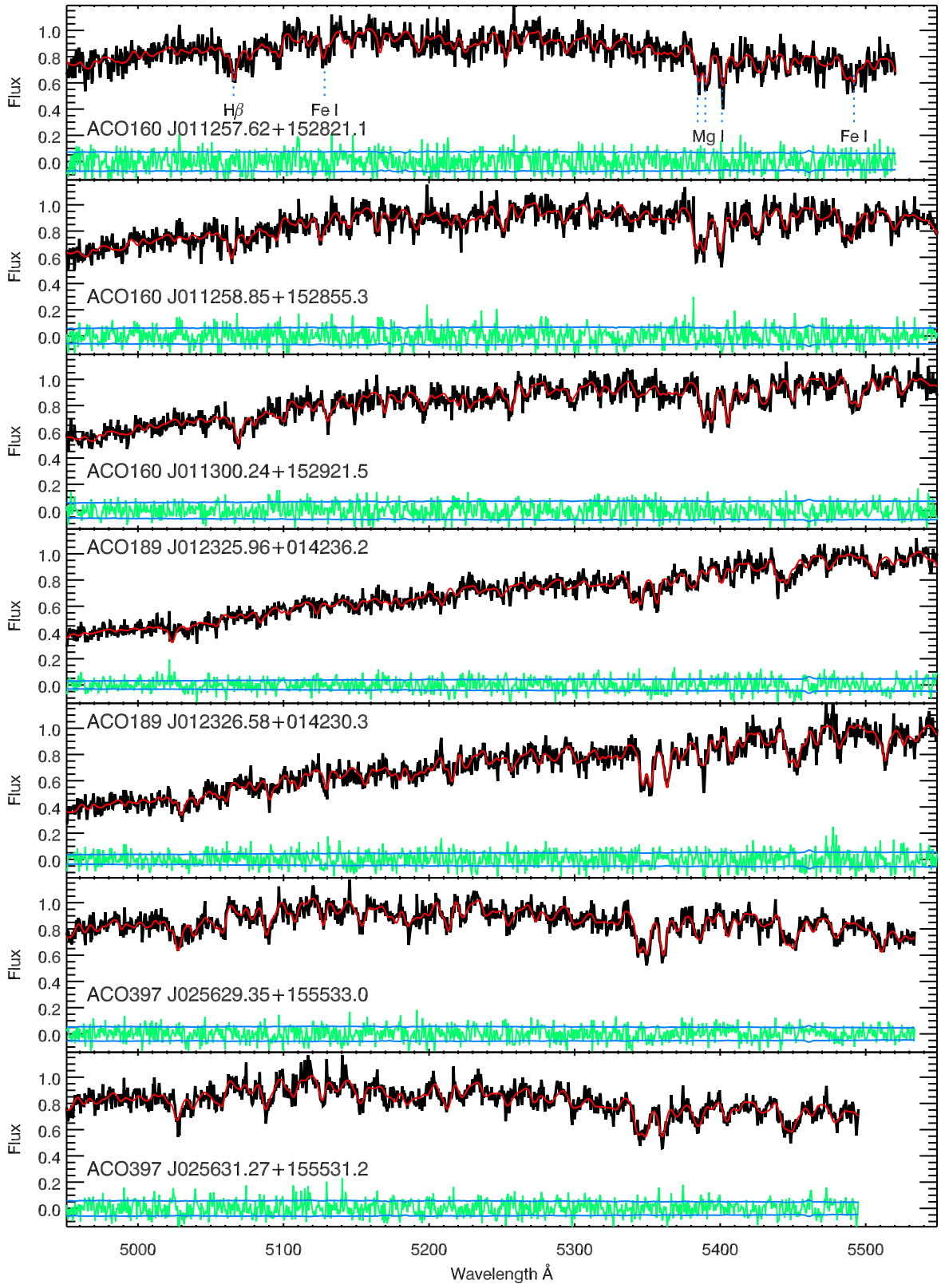

Figure S3: BTA spectra of 7 cE galaxies in Abell 160, Abell 189, and Abell 397. The best-fitting templates and fitting residuals are shown as red and green solid lines respectively. Flux uncertainties are shown in light blue